Fischer, Michael ; Angel, Ross J.

Accurate structures and energetics of neutral-framework zeotypes from dispersion-corrected DFT calculations

Journal Article	as:	published version (Version of Record)
DOI of this document*(secondary publication):		https://doi.org/10.26092/elib/2848
Publication date of this document:		07/03/2024

* for better findability or for reliable citation

Recommended Citation (primary publication/Version of Record) incl. DOI:

Michael Fischer, Ross J. Angel; Accurate structures and energetics of neutral-framework zeotypes from dispersion-corrected DFT calculations. J. Chem. Phys. 7 May 2017; 146 (17): 174111. https://doi.org/10.1063/1.4981528

Accurate structures and energetics of neutral-framework zeotypes from dispersion-corrected DFT calculations

Michael Fischer and Ross J. Angel

Citation: The Journal of Chemical Physics **146**, 174111 (2017); doi: 10.1063/1.4981528
View online: http://dx.doi.org/10.1063/1.4981528
View Table of Contents: http://aip.scitation.org/toc/jcp/146/17
Published by the American Institute of Physics

Accurate structures and energetics of neutral-framework zeotypes from dispersion-corrected DFT calculations

Michael Fischer[1,2,a] and Ross J. Angel[3]
[1]*Crystallography Group, Department of Geosciences, University of Bremen, Klagenfurter Straße 2-4, D-28359 Bremen, Germany*
[2]*MAPEX Center for Materials and Processes, University of Bremen, D-28359 Bremen, Germany*
[3]*Department of Geosciences, University of Padova, Via G. Gradenigo 6, I-35131 Padova, Italy*

(Received 2 February 2017; accepted 7 April 2017; published online 3 May 2017)

Density-functional theory (DFT) calculations incorporating a pairwise dispersion correction were employed to optimize the structures of various neutral-framework compounds with zeolite topologies. The calculations used the PBE functional for solids (PBEsol) in combination with two different dispersion correction schemes, the D2 correction devised by Grimme and the TS correction of Tkatchenko and Scheffler. In the first part of the study, a benchmarking of the DFT-optimized structures against experimental crystal structure data was carried out, considering a total of 14 structures (8 all-silica zeolites, 4 aluminophosphate zeotypes, and 2 dense phases). Both PBEsol-D2 and PBEsol-TS showed an excellent performance, improving significantly over the best-performing approach identified in a previous study (PBE-TS). The temperature dependence of lattice parameters and bond lengths was assessed for those zeotypes where the available experimental data permitted such an analysis. In most instances, the agreement between DFT and experiment improved when the experimental data were corrected for the effects of thermal motion and when low-temperature structure data rather than room-temperature structure data were used as a reference. In the second part, a benchmarking against experimental enthalpies of transition (with respect to α-quartz) was carried out for 16 all-silica zeolites. Excellent agreement was obtained with the PBEsol-D2 functional, with the overall error being in the same range as the experimental uncertainty. Altogether, PBEsol-D2 can be recommended as a computationally efficient DFT approach that simultaneously delivers accurate structures and energetics of neutral-framework zeotypes. *Published by AIP Publishing.* [http://dx.doi.org/10.1063/1.4981528]

I. INTRODUCTION

The benchmarking of density-functional theory (DFT) calculations, i.e., the critical comparison of DFT results against reference data from high-level quantum-chemical calculations or experiment, has become a very active field of research. Comparative benchmarking studies that assess the performance of different exchange-correlation functionals and/or dispersion correction schemes have been published for organic molecules and their complexes,[1–5] molecular crystals,[6,7] and inorganic solids.[8–15] While it is beyond the scope of this work to provide a complete overview of previous benchmarking efforts, the recent work of Tran *et al.* can serve as an instructive example:[15] These authors compared different functionals from rungs 1 to 4 of "Jacob's Ladder" of DFT and also considered the inclusion of a pairwise dispersion correction. On "Jacob's Ladder,"[16] the local-density approximation (LDA) constitutes the first rung, semilocal functionals that include a dependence on the density gradient are on the second rung (generalized gradient approximation—GGA), *meta*-GGA functionals form the third rung, and hybrid functionals containing a fraction of exact exchange correspond to the fourth rung. Using a portfolio of 40 different functionals without dispersion correction, plus 20 dispersion-corrected variants, Tran *et al.* predicted the lattice parameters, bulk moduli, and cohesive energies of 44 strongly bound solids (elements and binary crystals) and 5 weakly bound systems (rare gas crystals and layered solids). They found that some GGA-type functionals that were specifically designed for solids, such as the PBE functional for solids (PBEsol)[17] and Wu-Cohen (WC)[18] functionals, deliver an accuracy that is on par with the best-performing *meta*-GGA and hybrid functionals for the strongly bound solids. They also observed that the inclusion of a dispersion correction can improve the performance of those functionals that have a systematic tendency to overestimate the lattice parameters in their uncorrected form, e.g., for the PBE functional.[19] Finally, only the dispersion-corrected approaches were found to give a correct description of the weakly bound systems.

Motivated by the widespread interest in zeolites and structurally related materials (zeotypes), which find applications in gas separation, catalysis, and ion exchange, some previous studies have assessed the performance of DFT in reproducing the structure and/or relative stability (difference in lattice energy with respect to α-quartz, the thermodynamically stable form at ambient conditions) of all-silica zeolites. A systematic tendency to underestimate the relative

[a]Electronic mail: michael.fischer@uni-bremen.de

energies when using GGA or hybrid functionals without a dispersion correction was found by different groups.[20–22] A recent study by Román-Román and Zicovich-Wilson showed that a combination of the hybrid PBE0 functional with a Grimme-type D2 dispersion correction gives a fairly good prediction of the relative energies.[23] However, these authors also observed a systematic overestimation of the molar volume by the PBE0-D2 approach (i.e., the DFT-optimized unit cells were systematically too large). We previously studied the performance of different GGA-type functionals with and without dispersion correction for neutral-framework zeotypes with SiO_2 and $AlPO_4$ compositions.[24] In the context of that study, we compiled a set of 14 reference structures for which high-quality experimental crystal structure data are available (8 all-silica zeolites, 4 porous aluminophosphates (AlPOs), and 2 dense phases: α-quartz and α-berlinite). We then performed DFT structure optimizations, employing three different exchange-correlation functionals without dispersion correction (PBE, WC, and PBEsol)[17–19] and two dispersion-corrected variants of PBE, the PBE-D2 approach devised by Grimme[25] and the PBE-Tkatchenko and Scheffler (TS) approach developed by Tkatchenko and Scheffler.[26] All functionals without dispersion correction showed a systematic tendency to overestimate the lattice parameters, with a mean of signed errors (MSE, see below) between +0.07 Å and +0.15 Å, and RMSE (root mean square of relative error) values in the range of 0.7%–1.4%. The dispersion-corrected approaches, particularly PBE-TS, gave rather accurate predictions, with MSE and RMSE values in the range +0.05 Å and 0.5%, respectively. On the other hand, WC and PBEsol delivered T–O bond lengths (T = tetrahedral atoms: Si, Al, and P) that were in closer agreement with experiment than the PBE-based approaches. Regarding the T–O–T angles, neither approach performed fully satisfactorily, with systematic tendencies to overestimate (PBE, WC, and PBEsol) or underestimate (PBE-D2 and PBE-TS) the angles. Furthermore, the dispersion-corrected functionals were found to exaggerate the distortion of two additional zeolites with distorted six-ring windows (all-silica SOD and AST). This observation was explained as probably being the result of the overestimation of dispersion interactions between atoms that are close together but not directly bonded to each other. Finally, the relative stabilities with respect to α-quartz were assessed for four all-silica zeolites for which experimental enthalpies of transition are available. Here, PBE-TS overestimated the energy differences, whereas the relative energies predicted by PBE-D2 were surprisingly accurate. Qualitatively identical findings were reported in a benchmarking study that addressed a larger variety of dense SiO_2 polymorphs, but only two zeolites.[27] Interestingly, these authors found that the pairwise D2 and TS dispersion correction schemes outperformed more elaborate non-local van der Waals functionals.

It is the aim of the present work to improve upon our previous study[24] in various aspects: First, we consider a combination of the PBEsol functional with two different pairwise dispersion corrections. This is primarily motivated by the superior performance of PBEsol in reproducing experimental T–O bond lengths. Second, as we pointed out earlier, the comparison of DFT and experimental structure data is hampered by the fact that DFT neglects any thermal motion, whereas most experimental measurements were performed at room temperature (RT). In the current work, we include a semi-quantitative assessment of the effect of temperature on the structural parameters in order to assess whether the agreement of DFT and experiment improves or worsens if temperature effects are accounted for. Finally, we also study the relative stability of all-silica zeolites in much more depth, performing calculations for all frameworks for which experimental enthalpies of transition are available.

II. COMPUTATIONAL DETAILS

A. Reference data

In the first part of the study, the performance of the dispersion-corrected variants of PBEsol was assessed in detail for the previously mentioned set of reference structures of 14 SiO_2 and $AlPO_4$ frameworks. This set consists of two dense phases (α-quartz and α-berlinite), eight all-silica zeolites (CHA, FAU, FER, IFR, LTA, RTE, SAS, and TON frameworks, the framework type codes FTC follow the IZA database[28]), and four aluminophosphates (AEI, AEN, CHA, and ERI frameworks). The members of this set were chosen on the basis of several considerations, which are explained in detail in our previous work.[24] Among the most important requirements regarding the experimental crystal structure data are (1) (practically) ideal stoichiometry and the absence of structural disorder, (2) the availability of structure data for a calcined system, obtained at room temperature (or below RT), (3) no unrealistic T–O bond distances or O–T–O angles deviating strongly from the ideal tetrahedral angle, and (4) the absence of T–O–T angles of 180°. As in previous work, two additional all-silica zeolites with strongly distorted six-ring windows (SOD[29] and AST[30]) were also considered. As the errors in lattice parameters for these two systems are systematically larger, they were not included in the calculation of the overall errors but will be discussed separately.

In our previous work, relatively little emphasis was placed on the prediction of relative stability of all-silica zeolites with respect to α-quartz, the thermodynamically stable SiO_2 polymorph at ambient conditions.[24] It was observed, however, that the inclusion of a dispersion correction is absolutely necessary to arrive at reasonable relative energies, in line with previous findings by other groups.[23,27] A review article covering calorimetric studies reports enthalpies of transition ΔH_{trans} (with respect to α-quartz) for a total of 17 all-silica (or high-silica) zeolites,[31] with values of ΔH_{trans} ranging from 6.6 to 14.4 kJ mol^{-1} and typical uncertainties on the order of 1 kJ mol^{-1}. Of these 17 zeolites, four are members of our set of reference structures (CHA, FAU, FER, and IFR) and a fifth one is AST, one of the structures with distorted six-rings. Additional calculations with the PBEsol-D2 and PBEsol-TS functionals were performed for 11 of the remaining 12 systems: AFI, BEA, CFI, ISV, ITE, MEI, MEL, MFI, MTW, MWW, and STT. Only the EMT zeolite was omitted, since a relatively high content of framework Al was reported in the original study.[32] Furthermore, α-cristobalite was included as an additional non-porous silica polymorph. For a given all-silica system, the total DFT energy of α-quartz (per SiO_2 unit) was subtracted from the total DFT energy of the system in

question (per SiO_2 unit) to give an energy difference (= relative energy) ΔE_{DFT}. These relative energies were then directly compared to experimental enthalpies of transition ΔH_{trans}, in keeping with previous work.[23] Additional calculations of the vibrational properties for a few zeolites showed that this simplification is justified, as the correction for zero-point vibration and temperature effects for $T = 298$ K amounts to less than 1 kJ mol^{-1} per formula unit of SiO_2.

Figure 1 lists all members of the two reference sets used for structures and energetics, respectively, and visualizes the overlap between them. In the remainder of this work, all-silica zeolites are designated by their framework type code (adding the name or acronym where useful), whereas the framework type code is supplemented by the subscript "AlPO" for aluminophosphate zeotypes, e.g., AEN_{AlPO}. The references from which the experimental crystal structure data were taken are compiled in Tables I and II.

B. Setup of DFT calculations

All DFT calculations were carried out using the CASTEP code (version 7.01), which uses plane waves and pseudopotentials.[61] The calculations used on-the-fly generated ultrasoft pseudopotentials and an energy cutoff of 800 eV, which was found to give very well-converged total energies. All free structural parameters were optimized using a Broyden-Fletcher–Goldfarb-Shanno (BFGS) optimization algorithm. For most systems (except those with the largest unit cells), calculations with k-meshes of different size were compared in order to ensure the convergence of the results with respect to the number of k-points. Details on the k-meshes used, the convergence criteria employed in the optimizations, and sample CASTEP input files are supplied in the supplementary material.

C. The PBEsol-D2 and PBEsol-TS functionals

The PBEsol exchange-correlation functional was developed in 2008 by Perdew and co-workers.[17] PBEsol is a GGA-type functional that is based on the PBE functional but provides a better description of solids as it restores the density-gradient expansion over a wide range of density gradients. PBEsol was found to deliver accurate structural parameters (and, where investigated, elastic properties) for different inorganic solids, among them elements and binary crystals,[9,14,15]

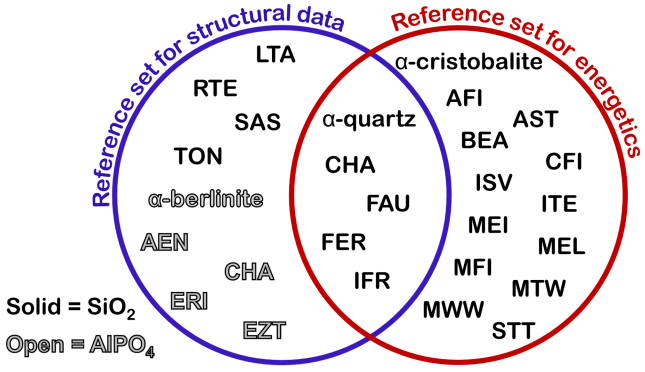

FIG. 1. Overview of reference sets used for the benchmarking against crystal structure data (left circle) and against enthalpies of transition (right circle).

TABLE I. Systems used in benchmarking against crystal structure data.

Framework type	Name or acronym	References
SiO_2 systems		
qtz	α-quartz	33
CHA	SiO_2-chabazite	34
FAU	Dealuminated zeolite Y	35
FER	SiO_2-ferrierite	36
IFR	ITQ-4	37
LTA	ITQ-29	38
RTE	RUB-3	39
SAS	SSZ-73	40
TON	ZSM-22	41
$AlPO_4$ systems		
qtz	α-berlinite	42
AEN	AlPO-53(B)	43
CHA	AlPO-34	44
ERI	AlPO-17	45
EZT	EMM-3	46

various minerals such as forsterite, pyrope, the Al_2SiO_5 polymorphs,[10–12] and sheet silicates,[13] while performing rather poorly for alkaline-earth metals.[9,15]

The pairwise D2 dispersion correction was proposed in 2006 by Grimme.[25] In this scheme, the total energy is given as

$$E_{total} = E_{el,DFT} + E_{disp}. \quad (1)$$

Here, $E_{el,DFT}$ is the electronic energy obtained from a DFT calculation using a given exchange-correlation functional and E_{disp} is the empirical dispersion energy obtained as

$$E_{disp} = -s_6 \sum_{i=1}^{N_{at}-1} \sum_{j=i+1}^{N_{at}} \frac{C_{6,ij}}{r_{ij}^6} f_{dmp}(r_{ij}). \quad (2)$$

In this equation, r_{ij} is the distance between a given pair of atoms, $C_{6,ij}$ is the dispersion coefficient for this pair of atoms, calculated using the geometric mean of atomic C_6 coefficients, s_6 is a global scaling factor, and f_{damp} is a damping function

TABLE II. Systems used in benchmarking against enthalpies of transition.

Framework type	Name or acronym	References
qtz	α-quartz	33
dia	α-cristobalite	47
AFI	SSZ-24	48 and 49
AST	Octadecasil	30
BEA	Beta	50 and 51
CFI	CIT-5	52
CHA	SiO_2-chabazite	34
FAU	Dealuminated zeolite Y	35
FER	SiO_2-ferrierite	36
IFR	ITQ-4	37
ISV	ITQ-7	53
ITE	ITQ-3	54
MEI	ZSM-18	55
MEL	ZSM-11	56
MFI	ZSM-5	57
MTW	ZSM-12	58
MWW	ITQ-1	59
STT	SSZ-23	60

that goes to zero for small interatomic distances to avoid an artificial dispersion contribution for atoms that are covalently bonded to each other. The damping function has the form

$$f_{damp}(r_{ij}) = \frac{1}{1 + \exp\left[-d\left(\frac{r_{ij}}{s_r(r_{vdW,i}+r_{vdW,j})} - 1\right)\right]}. \quad (3)$$

r_{vdW} are the van der Waals (vdW) radii of the ith and jth atom, s_r is a scaling factor by which the vdW radii are scaled, and d is a global factor determining the distance dependence of the correction. In Grimme's original work, values of $s_r = 1.10$ and $d = 20$ were recommended (note that the use of s_r was not included in the damping function given in Ref. 25, but all vdW radii presented in that publication were scaled by 1.10). Based on quantum-chemical calculations for isolated atoms, Grimme devised a consistent, generic set of atomic C_6 coefficients and vdW radii for all elements up to Xe.[25] The scaling factor s_6 in Equation (2) was optimized for different exchange-correlation functionals by minimising the error in interaction energies with respect to reference data for a set of 40 non-covalently bound complexes. The resulting s_6 values range from 0.75 for PBE to 1.25 for B97-D. It was later argued that a scaling of the dispersion energy by a constant factor s_6 also affects the dispersion contribution for large interatomic distances, which should be effectively independent of the exchange-correlation functional.[62]

A combination of PBEsol with the Grimme-type D2 dispersion correction scheme was proposed by Csonka and co-workers, shortly after the publication of the PBEsol functional.[63] In contrast to the original implementation of the D2 correction, which uses a common value of s_r but different values of s_6 for different exchange-correlation functionals, these authors fixed s_6 to unity, but adjusted s_r in order to reproduce high-level (coupled-cluster singles and doubles plus perturbative triples (CCSD(T))) interaction energies from the S22 set of organic dimers.[64] The optimized PBEsol-D2 functional, which uses $s_r = 1.42$, was then applied to large organic molecules, for which it was found to be relatively accurate given the modest computational expense. Further work on the Grimme-type dispersion correction method led to the development of the D3 scheme, which includes a coordination-dependent calculation of the dispersion coefficients as well as a three-body term.[65] The D3 correction was first used in conjunction with the PBEsol functional by Goerigk and Grimme.[1] Due to technical limitations, PBEsol-D3 could not be tested in the context of the present study. It should be noted, however, that previous studies that assessed the performance of both the D2 and the D3 schemes (in combination with PBE) for the calculation of adsorption energies of small molecules in zeolites[66,67] or for the prediction of relative energies and densities of hybrid zeolitic imidazolate frameworks (ZIFs)[68] reported very similar results for both approaches.

The TS dispersion correction scheme was introduced in 2009 by Tkatchenko and Scheffler.[26] Like the previously described D2 scheme, this is also a pairwise dispersion correction method, in which the dispersion contribution is calculated according to Equation (2). However, unlike the D2 scheme, which uses a fixed set of atomic C_6 coefficients, the TS scheme scales the dispersion coefficients and the vdW radii by the ratio of the effective volume of an atom in the system of interest (molecule and solid) to the volume of the free atom. The effective volume is determined using a Hirshfeld partitioning of the DFT electron density.[69,70] There is no scaling of the overall dispersion energy, i.e., the factor s_6 from Equation (2) is unity. The damping function corresponds to Equation (3), where the factor s_r can be varied for different exchange-correlation functionals (as in the D2 scheme, $d = 20$). In the original work of Tkatchenko and Scheffler, a value of 0.94 was determined for a combination of the TS scheme with the PBE functional. This value was obtained by minimising the error of the PBE-TS interaction energies with respect to reference data from the S22 set of organic dimers.[64] PBE-TS has been found to give excellent agreement with experimental structures for various molecular crystals[6] and for different sheet silicates.[13] Furthermore, it was the best-performing approach in terms of accurate lattice parameters in our previous benchmarking study of neutral-framework zeotypes, with PBE-D2 being a close second.[24] On the other hand, PBE-TS does not deliver satisfactory results for ionic solids, and it has been shown that this shortcoming can be remedied by replacing the standard Hirshfeld partitioning of the electron density by an iterative Hirshfeld (HI) partitioning scheme.[71]

A combination of the TS scheme with the PBEsol functional was introduced by Al-Saidi and co-workers.[72] These authors used the same method to determine s_r as Tkatchenko and Scheffler and arrived at an optimal value of 1.06. They went on to compare the performance of PBEsol-TS to some other dispersion-corrected DFT approaches for rare-gas crystals, molecular crystals, and layered solids and observed a reasonable prediction of lattice parameters (on par with PBE-TS), but a pronounced underestimation of cohesive energies by PBEsol-TS.

D. Assessment of errors

In order to quantify the agreement between DFT calculations and experiment, the error in a quantity x was calculated as

$$err_x = x_{DFT} - x_{exp}. \quad (4)$$

In the benchmarking against experimental structure data, errors in lattice parameters, T–O bond lengths, and T–O–T angles were evaluated. For the study of relative stabilities, $x_{DFT} = \Delta E_{DFT}$ and $x_{exp} = \Delta H_{trans}$. In order to obtain the overall error (e.g., in lattice dimensions) from the individual errors err_x, the mean of signed errors (MSEs) was calculated as

$$\mathrm{MSE} = \frac{1}{N_i}\sum_{i=1}^{N_i} err_{x,i}. \quad (5)$$

The mean of signed errors is very helpful to identify systematic over- or underestimations. On the other hand, even large individual errors will compensate each other if they have different signs. Hence, the mean of absolute errors (MAEs) is a useful complementary measure of the overall deviation,

$$\mathrm{MAE} = \frac{1}{N_i}\sum_{i=1}^{N_i} \left|err_{x,i}\right|. \quad (6)$$

For lattice parameters and energetics, relative deviations were evaluated in addition to the absolute errors. Here, the root mean square of relative errors (RMSEs) was calculated as

$$\mathrm{RMSE}\,[\%] = \sqrt{\frac{1}{N_i}\sum_{i=1}^{N_i}\left(100\cdot\frac{err_{x,i}}{x_{exp,i}}\right)^2}. \qquad (7)$$

In the present study, the structural parameters of the DFT-optimized structures were directly compared to experimental values, which were—in most cases—obtained at room temperature (RT). Since DFT delivers the equilibrium structure at 0 K, certain differences in structural parameters have to be expected: For example, the experimental lattice parameters will be affected by thermal expansion. Since a complete correction for these effects is not possible due to the lack of available experimental data, the initial benchmarking of DFT against experiment will make use of the published crystal structures without any corrections. Subsequently, it will be discussed how the agreement in lattice parameters changes if low-temperature (LT) data, rather than RT data, are used as a reference (these are available for a few systems), and a correction of the T–O bond lengths for thermal motion will be applied where possible.

III. RESULTS AND DISCUSSION

A. Structural parameters of all-silica zeolites and aluminophosphates

1. Lattice parameters

In our previous benchmarking study, the errors in lattice parameters were evaluated separately for the SiO_2 and $AlPO_4$ systems of the set of reference structures.[24] Since that work showed that the observed trends in the errors are identical for both groups, all systems were evaluated together in the present study. This analysis delivers one overall value of MSE, MAE, and RMSE for each functional. While the individual results are given in the supplementary material, the resulting overall errors, as well as the largest individual errors (both positive and negative errors in absolute and relative terms), obtained for PBEsol-D2 and PBEsol-TS are compiled in Table III. For comparison, values for PBEsol and dispersion-corrected versions of the PBE functional (PBE-D2 and PBE-TS) from our previous work are also included. Figure 2 visualizes the MSE and MAE for these five functionals. It has to be noted that this analysis considers only the lattice dimensions *a*, *b*, and *c*. For the monoclinic systems, the errors in the monoclinic angles delivered by PBEsol-D2 and PBEsol-TS are always small, not exceeding 0.2°. As errors of this magnitude are on the same scale as typical experimental uncertainties, they can be considered insignificant in the context of the present work.

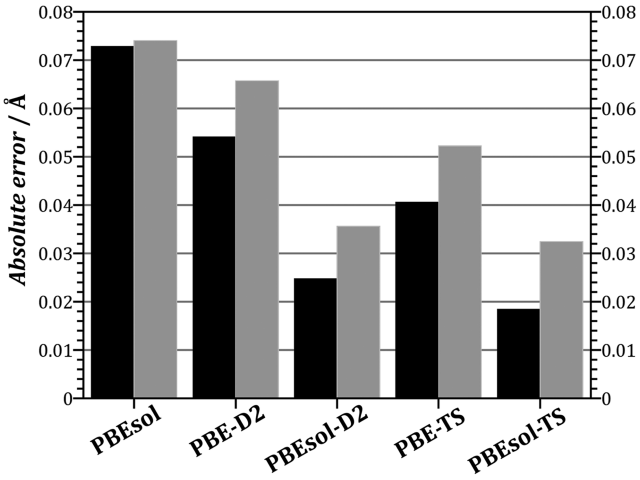

FIG. 2. MSE (black) and MAE (grey) in lattice parameters obtained with different DFT approaches.

The positive values of MSE indicate that all five functionals tend to overestimate the lattice parameters. However, while this tendency is pronounced for uncorrected PBEsol, the inclusion of a dispersion correction term reduces it quite drastically. With values of +0.025 Å and +0.018 Å, respectively, the MSEs of PBEsol-D2 and PBEsol-TS are about 40% to 50% smaller than that of PBE-TS, the best-performing approach of our previous study. A similar reduction in the errors is found in the values of MAE (which range close to 0.035 Å, 30% to 40% smaller than that for PBE-TS) and of RMSE (which are close to 0.3%, a reduction of roughly 30% with respect to PBE-TS). Thus, all three quantities employed to assess the overall error agree that the dispersion-corrected variants

TABLE III. Overall errors in lattice parameters obtained with PBEsol-D2 and PBEsol-TS functionals and comparison to selected previous results.[24] The largest individual errors found among all systems are also given: LSE± = largest signed positive/negative error; LRE± = largest relative positive/negative error.

	PBEsol	PBE-D2	PBEsol-D2	PBE-TS	PBEsol-TS
MSE (Å)	+0.073	+0.054	+0.025	+0.041	+0.018
MAE (Å)	0.074	0.066	0.036	0.052	0.032
LSE+ (Å)	+0.172 (*b*, TON)	+0.265 (*a*, AEN_{AlPO})	+0.082 (*a*, TON)	+0.169 (*a*, AEN_{AlPO})	+0.077 (*a*, ERI_{AlPO})
LSE– (Å)	–0.019 (*b*, IFR)	–0.119 (*b*, AEN_{AlPO})	–0.072 (*c*, CHA_{AlPO})	–0.093 (*b*, AEN_{AlPO})	–0.085 (*c*, CHA_{AlPO})
RMSE (%)	0.69	0.58	0.34	0.47	0.32
LRE+ (%)	+1.39 (*c*, TON)	+1.47 (*a*, AEN_{AlPO})	+0.69 (*c*, SAS)	+1.09 (*a*, ERI_{AlPO})	+0.66 (*c*, SAS)
LRE– (%)	–0.14 (*b*, IFR)	–0.85 (*b*, AEN_{AlPO})	–0.48 (*c*, CHA_{AlPO})	–0.67 (*b*, AEN_{AlPO})	–0.57 (*c*, CHA_{AlPO})

TABLE IV. Overall errors in T–O bond lengths obtained with PBEsol-D2 and PBEsol-TS functionals and comparison to selected previous results.[24] Largest individual errors are also given.

	Exp	PBEsol	PBE-D2	PBEsol-D2	PBE-TS	PBEsol-TS
Si–O bonds						
d_{aver} (Å)	1.601	1.609	1.615	1.608	1.614	1.608
MSE (Å)		+0.008	+0.014	+0.007	+0.013	+0.007
MAE (Å)		0.010	0.015	0.010	0.014	0.010
LSE (Å)		+0.032	+0.039	+0.031	+0.038	+0.031
Al–O bonds						
d_{aver} (Å)	1.722	1.733	1.738	1.731	1.737	1.731
MSE (Å)		+0.011	+0.016	+0.009	+0.015	+0.009
MAE (Å)		0.021	0.023	0.021	0.022	0.021
LSE (Å)		+0.074	+0.083	+0.070	+0.082	+0.069
P–O bonds						
d_{aver} (Å)	1.528	1.523	1.529	1.522	1.528	1.522
MSE (Å)		−0.005	0.001	−0.006	0.000	−0.006
MAE (Å)		0.017	0.017	0.017	0.016	0.017
LSE (Å)		−0.058	−0.055	−0.060	−0.056	−0.060

of PBEsol constitute a significant improvement over the performance of the previously recommended PBE-TS. Among the two approaches, PBEsol-TS is somewhat superior to PBEsol-D2, a behavior that mirrors the better performance of PBE-TS compared to PBE-D2.

In addition to the analysis of the overall errors, it is also insightful to look at the largest individual errors, which are included in Table III. First of all, it is worth noting that the largest positive and negative deviations have a similar magnitude (both in absolute and relative terms), corroborating that PBEsol-D2 and PBEsol-TS exhibit a very "balanced" behavior. Second, the largest individual errors are significantly smaller than those for the dispersion-corrected variants of PBE. Particularly remarkable differences are found for AEN_{AlPO}, where both PBE-D2 and PBE-TS perform poorly, overestimating the length of a and underestimating the length of b. As discussed in the previous study, this is related to an exaggerated distortion of an elliptically distorted eight-ring window in this structure. In contrast, PBEsol-D2 and PBEsol-TS do not show unusually large deviations for AEN_{AlPO}. Altogether, the systematic reduction of the largest individual errors confirms the superior performance of these functionals.

2. T–O bond lengths and T–O–T angles

The average Si–O, Al–O, and P–O bond lengths, the overall errors MSE and MAE, and the largest individual errors LSE that were obtained with dispersion-corrected variants of PBEsol are compiled in Table IV. As a first observation, it can be noted that PBEsol-D2 and PBEsol-TS deliver practically identical results to PBEsol, since the inclusion of a dispersion correction has virtually no impact on the equilibrium distances between atoms that are directly bonded to each other. Figure 3 shows histogram plots detailing the frequency of occurrence of Si–O, Al–O, and P–O bond lengths in the structures optimized with PBEsol-D2 in comparison to the experimental distribution (T–O bond lengths obtained with PBEsol-TS are not shown because the results are practically identical to those obtained with PBEsol-D2). Due to its tendency to optimize all bonds of a given type towards an equilibrium value, DFT delivers a much narrower distribution of the bond lengths than experiment. A comparison of the average bond lengths to experimental values points to a systematic tendency to overestimate Si–O bond lengths (modestly, by less than +0.010 Å) and Al–O bond lengths (more prominently), whereas the P–O distances are somewhat underestimated. The overall deviations as measured by the mean of absolute errors are significantly smaller for Si–O bond lengths, with MAE around 0.010 Å, than for the other two types of bonds, for which the values of MAE are closer to 0.020 Å. However, as is clearly visible from Figure 3, the variation of the experimental bond distances—which is likely to reflect, at least partly, a limited quality of the data used in the structure refinements—is also considerably larger for Al–O and P–O bond lengths, and it is thus not surprising that the average deviations are increased due to the larger scatter in experimental bond lengths. The largest individual errors occur for T–O distances that are unusually short in the case of Si–O

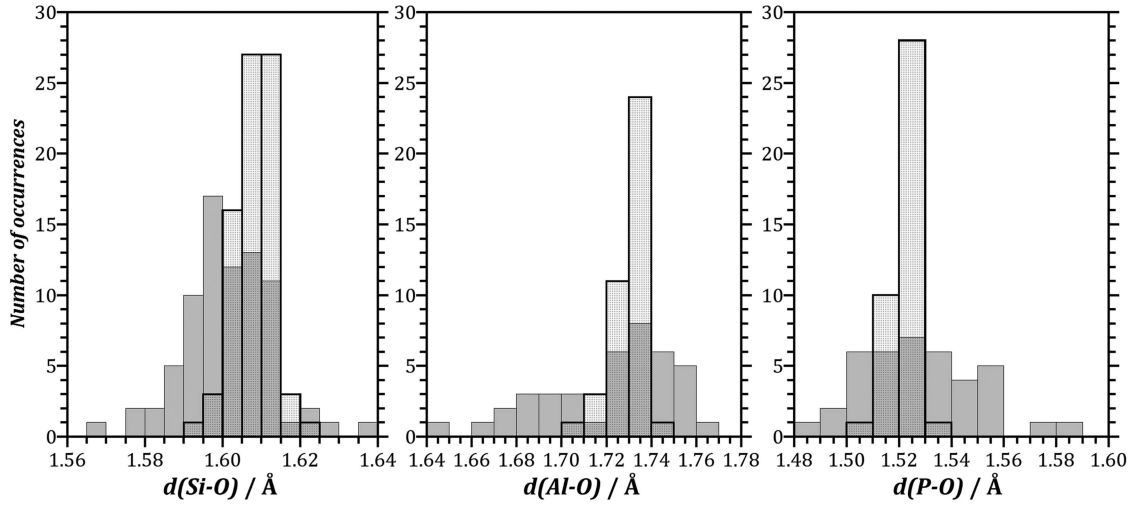

FIG. 3. Histogram of T–O bond distances found in experimental structures (grey, solid columns) and in structures optimized with PBEsol-D2 (semi-transparent columns).

TABLE V. Overall errors in T–O–T angles obtained with PBEsol-D2 and PBEsol-TS functionals and comparison to selected previous results.[24] Largest individual errors are also given.

	Expt.	PBEsol	PBE-D2	PBEsol-D2	PBE-TS	PBEsol-TS
Si–O–Si angles						
ω_{aver} (deg)	149.86	150.36	148.17	149.23	148.07	149.01
MSE (deg)		+0.50	−1.69	−0.63	−1.79	−0.85
MAE (deg)		1.49	2.62	1.85	2.46	1.98
LSE (deg)		−5.43	−8.81	−5.75	−9.05	−5.98
Al–O–P angles						
ω_{aver} (deg)	147.48	148.83	147.31	147.82	146.82	147.74
MSE (deg)		+1.35	−0.17	+0.34	−0.66	+0.26
MAE (deg)		2.68	2.45	2.16	2.60	2.17
LSE (deg)		−7.10	7.45	−7.91	7.39	−7.86

and Al–O bonds (Si1-O1 in RTE, $d_{exp} = 1.577$ Å, Al1-O2 in AEN_{AlPO}, $d_{exp} = 1.650$ Å) and unusually long in the case of P–O bonds (P2-O11 in AEN_{AlPO}, $d_{exp} = 1.576$ Å), in line with the aforementioned tendencies of DFT to (a) overestimate Si–O and Al–O distances and underestimate P–O distances and (b) give a narrower bond length distribution. For Si–O and Al–O bond lengths, all PBEsol-based approaches perform significantly better than those based on PBE, which overestimate the distances more strongly.

The average Si–O–Si and Al–O–P angles as well as MSE, MAE, and the largest individual errors in these angles are compiled in Table V. While PBEsol delivers on average somewhat larger Si–O–Si angles than observed experimentally, all dispersion-corrected approaches have a tendency to underestimate these angles. Compared to PBE-D2 and PBE-TS, this systematic deviation is reduced for the PBEsol-D2 and PBEsol-TS, with values of MSE that are roughly half as large. The MAE values are also smaller, but still substantial (in the range of 2°). A reduction of the mean of absolute errors is also found when moving from the PBE-based to the PBEsol-based approaches for the Al–O–P angles; in this case, however, there is no evidence for a systematic overestimation of the angles (MSE close to zero).

3. Influence of temperature on the structural parameters—A partial assessment

In the analysis presented in Secs. III A 1 and III A 2, experimental crystal structures were taken as reference data without further corrections. We have to note, however, that these structures were mostly determined at room temperature (except for IFR (ITQ-4),[37] TON (ZSM-22),[41] and AlPO-34 (CHA),[44] for which the structures were obtained at lower temperatures), whereas the DFT-optimized structures correspond to the equilibrium structure at absolute zero. On the one hand, there should thus be a certain difference in lattice parameters due to (positive or negative) thermal expansion. On the other hand, it has been shown that thermal vibrations lead to a shortening of the "apparent" (experimentally observed) T–O bond distances in tetrahedral frameworks.[73] It could now be speculated that the excellent performance of PBEsol-D2 and PBEsol-TS found above is, at least in part, an artifact of comparing the DFT-optimized structures to experimental RT data. While the available experimental data do not allow for a complete assessment of these effects, a partial analysis for selected systems is presented here.

Regarding the influence on the lattice parameters, such a partial assessment can be made by considering those systems where the low-temperature thermal expansion has been studied experimentally. Such measurements have been performed for all-silica zeolites with topologies FAU,[74] IFR (ITQ-4),[37] and LTA (ITQ-29),[75] as well as AlPO-34 (CHA_{AlPO})[44] and AlPO-17 (ERI_{AlPO}),[45] all of which exhibit negative thermal expansion (NTE), whereas a qualitative change in thermal expansion upon heating has been observed for all-silica FER (positive thermal expansion up to 400 K, NTE above that temperature).[76] For these six systems, the lattice parameters measured at RT and at lower temperatures (between 18 and 150 K) are supplied in the supplementary material (Table 10), together with the DFT-optimized lattice parameters obtained with PBEsol-D2 and PBEsol-TS. The differences between RT and LT lattice parameters range from less than 0.02 Å to around 0.06 Å (reaching up to 0.5% in relative terms). A comparison with the DFT results shows that the DFT-optimized lattice parameters are in better agreement with the LT data in many instances, most markedly for a in IFR and ERI_{AlPO}, systems that show pronounced negative thermal expansion in this direction. While the opposite trend is also observed in a number of cases, a calculation of the MSE and MAE for this subset of structures delivers significantly smaller values when the LT lattice parameters are used as a reference (Table VI). This observation corroborates that the good performance of dispersion-corrected PBEsol is not an artifact of the use of RT structures as reference data. On the contrary, the agreement between DFT and experiment should become even better if high-quality LT data were available for all frameworks.

In framework silicates, thermal vibrations lead to correlated motions of SiO_4 tetrahedra with much larger amplitudes of vibration than the bond-stretching vibrations. As a consequence, the average positions of the oxygen atoms at finite temperature, as measured by diffraction experiments, are closer to the silicon atoms than the true equilibrium position (Figure 4). This leads to a contraction of the "apparent" Si–O bond lengths,[73,77] which becomes more pronounced with increasing temperature as the librational motion of the tetrahedra increases: For example, the experimentally observed, uncorrected Si–O bond distances in albite decrease from 1.603 Å at cryogenic temperatures to 1.595 Å at 1200 K.[73] However, a correction using the TLS model (accounting for translational, librational, and screw modes) delivers bond lengths that increase from 1.605 Å to 1.627 Å across this range of temperatures. Thus, the effect of the correlated motion on the

TABLE VI. MSE and MAE in lattice parameters calculated for a set of six frameworks for which lattice parameters obtained at different temperatures are available, using either room-temperature (RT) or low-temperature (LT) experimental data as a reference.

	PBEsol-D2	PBEsol-TS
MSE (RT) (Å)	+0.033	+0.026
MSE (LT) (Å)	+0.018	+0.011
MAE (RT) (Å)	0.043	0.040
MAE (LT) (Å)	0.035	0.031

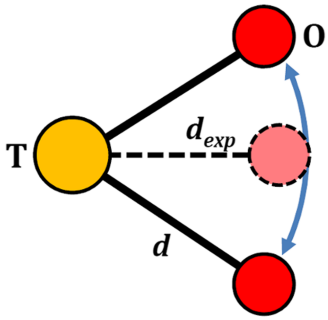

FIG. 4. Visualization of the difference between true and "apparent" bond lengths: The dominant motion of the TO_4 tetrahedron is a rotation around its center. The oxygen atom therefore traverses an arc in space (blue arrow). The time-averaged position of the oxygen atom (dashed circle), which is determined by diffraction, lies closer to the Si atom than its true position at any point in time. Therefore, the experimentally measured distance d_{exp} is shorter than the true distance d.[73,77] For clarity, the diagram shows only a single T–O bond, rather than a T–O–T linkage (also see Figure 5 of Ref. 73).

"apparent" bond lengths is so large that it masks the thermal expansion of the Si–O bonds entirely. While the magnitude of the correction is relatively modest for RT structures (see below), the experimental bond lengths should be corrected in order to make them directly comparable to the DFT results. Since the full TLS correction requires elaborate calculations, a simpler formula to correct the "apparent" T–O bond lengths for the effects of thermal motion was proposed by Downs *et al.*[73] In this "Simple Rigid Body" (SRB) correction, a term is added to the uncorrected bond length, the magnitude of which depends on the difference between the isotropic displacement parameters B_{iso} of the atoms participating in the bond. It was shown in the original work for a set of silicates that the SRB correction formula gives results that are in good agreement with the more elaborate TLS correction.

When testing the applicability of the SRB correction for our set of reference structures, it was found that reasonably meaningful correction terms were obtained for no more than six of the 14 systems due to insufficient data quality. In the other eight cases, either one global value of B_{iso} was given for all atoms in the structure (leading to an SRB correction of zero) or the scatter in the B_{iso} values was so large that $B_{iso}(\mathrm{T}) > B_{iso}(\mathrm{O})$ for some combinations of atoms, rendering the SRB correction meaningless. For the remaining six systems, individual values of B_{iso} for all non-equivalent atoms were available in four cases (α-quartz, α-berlinite, FAU, and FER), whereas only element-specific displacement parameters were given in the cases of RTE and $\mathrm{AEN_{AlPO}}$.

The average uncorrected and SRB-corrected T–O bond lengths are compiled in Table VII (individual results are given in the supplementary material). For the dense systems, α-quartz and α-berlinite, the changes in the average bond lengths due to the SRB correction are virtually identical, amounting to +0.006 Å. For the zeotypes, the increase in the average bond lengths is usually larger, reaching up to +0.016 Å for the Al–O bonds in $\mathrm{AEN_{AlPO}}$. The only exception is RTE, for which a very small correction of +0.002 Å is found. In the view of the rather large scatter of the SRB corrections for the porous frameworks, the main conclusion that we can draw at this stage is that a correction for temperature effects will lead to an increase in the experimental bond length that is likely

TABLE VII. Average "apparent" T–O bond lengths d_{exp} and SRB-corrected bond lengths $d_{exp,SRB}$, calculated for those systems where sufficient data to apply the SRB correction are available. The last column gives the difference Δd between the two values.

	d_{exp} (Å)	$d_{exp,SRB}$ (Å)	Δd (Å)
Si–O bonds			
α-quartz	1.609	1.615	0.006
FAU	1.606	1.615	0.009
FER	1.595	1.610	0.015
RTE	1.601	1.603	0.002
Al–O bonds			
α-berlinite	1.734	1.740	0.006
$\mathrm{AEN_{AlPO}}$	1.717	1.733	0.016
P–O bonds			
α-berlinite	1.526	1.532	0.006
$\mathrm{AEN_{AlPO}}$	1.534	1.543	0.009

to be—on average—somewhat larger than that for the dense phases. As we have seen above, DFT calculations with PBEsol (with or without dispersion correction) deliver Si–O and Al–O bond lengths that are larger than the uncorrected experimental values, with MSEs of approximately +0.007 Å and +0.010 Å, respectively (Table IV). We can thus anticipate that the overall agreement between DFT and experiment should become better if sufficient data were available to apply the SRB correction to all Si–O and Al–O bond lengths. On the other hand, the P–O bond distances are already underestimated by the calculations (MSE of −0.006 Å), and a correction for temperature effects would make matters worse. We can only speculate that this may be due to an overestimation of the covalent character of the P–O bond in the DFT calculations. In any case, it is an issue that should be addressed in future work. As a final remark, it has to be reiterated that the analysis presented here is necessarily a preliminary one, mainly due to the lack of structures with sufficiently accurate displacement parameters in the reference set. A complete assessment of the effects of temperature on bond lengths in neutral-framework zeotypes would require new diffraction measurements on high-quality samples to allow anisotropic displacement parameters to be determined for every independent atom.

4. Strongly distorted structures

In our previous benchmarking study,[24] we observed a qualitatively different behavior of GGA functionals with and without dispersion correction in the description of two all-silica zeolites with strongly distorted six-ring windows, all-silica SOD and AST: While the functionals without dispersion correction gave less distorted structures compared to experiment, the dispersion-corrected variants overestimated the distortion. The errors in the lattice parameters reached up to six per cent, which is why these "outliers" were not included in the set of reference structures. In the context of the present work, optimizations with the PBEsol-D2 and PBEsol-TS functional were performed for all-silica SOD and AST. The resulting lattice parameters and T–O–T angles are given in Table VIII. The dispersion-corrected variants of PBEsol behave qualitatively identical to PBE-D2 and PBE-TS, underestimating c and both

TABLE VIII. Selected results obtained for systems with strongly distorted six-rings, all-silica SOD and AST. Some results from previous work are given for comparison.[24]

		Expt.	PBEsol	PBE-D2	PBEsol-D2	PBE-TS	PBEsol-TS
SOD	a (Å)	12.441	12.597	12.442	12.429	12.410	12.406
	err_{rel} (%)		1.3	0.0	−0.1	−0.2	−0.3
	c (Å)	7.091	7.411	6.915	6.984	6.898	6.934
	err_{rel} (%)		4.5	−2.5	−1.5	−2.7	−2.2
	ω(Si1−O1−Si1) (deg)	149.02	155.90	145.73	147.13	144.40	146.25
	ω(Si1−O2−Si1) (deg)	145.93	150.64	141.74	143.46	142.49	142.70
AST	a (Å)	9.255	9.387	9.115	9.127	9.066	9.095
	err_{rel} (%)		1.4	−1.5	−1.4	−2.0	−1.7
	c (Å)	13.501	13.556	13.739	13.660	13.757	13.673
	err_{rel} (%)		0.4	1.8	1.2	1.9	1.3
	ω(Si1−O1−Si1) (deg)	147.22	147.65	149.74	149.33	150.03	149.52
	ω(Si1−O2−Si1) (deg)	146.54	147.50	143.03	143.75	142.18	143.30
	ω(Si1−O3−Si2) (deg)	151.74	156.23	145.89	147.25	144.93	146.40

T–O–T angles in the case of SOD, and overestimating a while underestimating c and two of the three T–O–T angles for AST. However, the magnitude of the errors is slightly reduced for PBEsol-D2 and PBEsol-TS. As discussed in detail in the context of our previous study (especially Figure 8 of Ref. 24), the observed deviations are directly linked to an exaggeration of the distortion of irregular six-ring windows in these structures. We explained this behavior with an overestimation of dispersion interactions between atoms that are close together, but not directly linked to each other, e.g., between oxygen atoms on both sides of the distorted window. Since the predicted over-stabilization of the distortion persists when changing the exchange-correlation functional, it appears that this may be a systematic shortcoming of pairwise dispersion correction schemes.

B. Relative stability of all-silica zeolites

First of all, we briefly assess the agreement of the DFT-optimized lattice parameters with experimental data for those all-silica systems from the reference set for energetics that have not been covered in Secs. III A 1–III A 4 (all systems from the right-hand side of Figure 1 except AST). These lattice parameters, as well as the individual relative deviations in per cent, are compiled in Table 13 of the supplementary material. We observe excellent agreement for 5 out of 12 systems (AFI, BEA, ITE, MFI, and MTW), with all relative deviations in lattice parameters being no larger than 0.5%. Agreement is good to fair for another 6 systems (α-cristobalite, CFI, ISV, MEL, MWW, and STT), where relative deviations in at least one individual parameter are larger than 0.5% but do not (significantly) exceed 1.0%. The largest relative errors are found for MEI (ZSM-18), where the length of c is underestimated by approximately −1.4%, and a is also moderately shorter than in the experimental structure (by −0.6%). For this system, it has to be noted that the only available experimental lattice parameters were obtained for a sample that contained a significant amount of framework Al atoms and charge-balancing cations.[55] This renders a comparison to the all-silica model used in the computations problematic. If the results for MEI are excluded, a calculation of the overall errors (omitting monoclinic angles) delivers MSE values of +0.037 Å (PBEsol-D2) and +0.023 Å (PBEsol-TS), MAE values of 0.050 Å (PBEsol-D2) and 0.054 Å (PBEsol-TS), and RMSE values of 0.43% (PBEsol-D2) and 0.46% (PBEsol-TS).

Having thus corroborated our previous conclusion that dispersion-corrected variants of PBEsol predict the lattice parameters of all-silica frameworks with high accuracy, we now turn our attention to the prediction of the relative energies (with respect to α-quartz). The left-hand side of Figure 5 shows ΔE_{DFT} as a function of the framework density FD for all systems from the reference set for energetics (16 all-silica zeolites and α-cristobalite, see Figure 1) for PBEsol-D2 and PBEsol-TS. A trendline representing the correlation between FD and the experimental enthalpies of transition ΔH_{trans} is also shown. Qualitatively, both functionals reproduce the experimental trend. However, the PBEsol-TS functional tends to overestimate the relative energy for a given framework density, whereas the PBEsol-D2 data points fall much closer to the trendline.

The good performance of PBEsol-D2 and the systematic overestimation of the relative energies by PBEsol-TS are also evident when plotting ΔE_{DFT} against the experimental values of ΔH_{trans} (Figure 5, right). To enable a quantitative assessment, the overall errors MSE, MAE, and RMSE were calculated. These are compiled in Table IX. For PBEsol-D2, the small MSE of +0.75 kJ mol^{-1} together with the similar (absolute) magnitude of the largest positive and negative individual errors corroborates the absence of a significant systematic error. With 1.1 kJ mol^{-1}, the mean of absolute errors is in the same range as the typical uncertainty in the experimental enthalpies of transition of approximately 1 kJ mol^{-1}.[31] The systematic overestimation of the relative energies by PBEsol-TS manifests in a much larger MSE of +2.5 kJ mol^{-1} and in MSE and MAE values of almost equal magnitude. Consequently, the RMSE of PBEsol-TS is also much larger (33%) than that of PBEsol-D2 (17%). Since both approaches use the same exchange-correlation functional, it is obvious that their significantly different performance for the relative energies can only be attributed to the influence of the dispersion correction scheme. Apparently, the TS dispersion correction in its

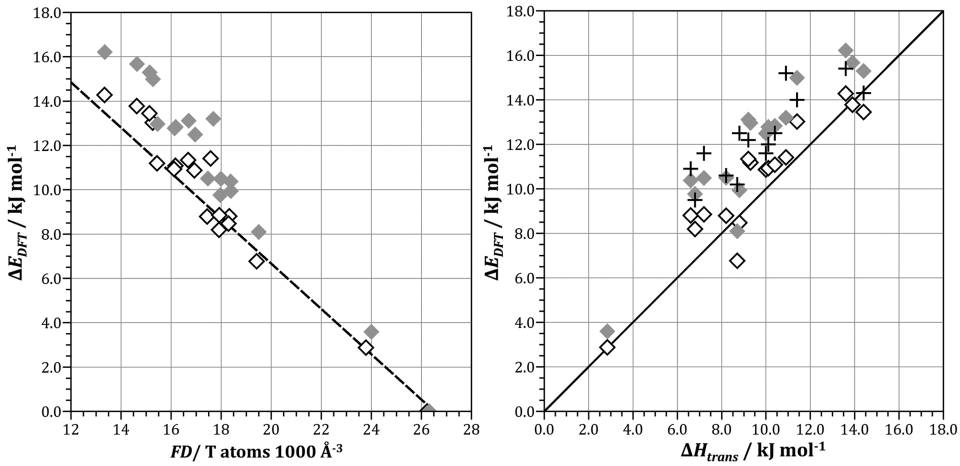

FIG. 5. Left: Correlation between framework density *FD* and relative energy ΔE_{DFT} as obtained from calculations with PBEsol-D2 (open diamonds) and PBEsol-TS (grey diamonds). The dashed line corresponds to the correlation between *FD* and ΔH_{trans} calculated on the basis of experimental data from Ref. 31. Right: Plot of relative energy ΔE_{DFT} against experimental enthalpy of transition ΔH_{trans} for PBEsol-D2 (open diamonds) and PBEsol-TS (grey diamonds). Results from a previous computational study employing the PBE0-D2 functional are included for comparison (crosses).[23]

implementation optimized for PBEsol overestimates the long-range dispersion interactions, leading to an overstabilization of the dense phases and thus a larger range of ΔE_{DFT} values. The same observation was made when comparing the relative energies obtained with PBE-D2 and PBE-TS for a subset of all-silica zeolites in our previous work.[24] We will return to this aspect in Sec. III C.

The right-hand side of Figure 5 also contains the PBE0-D2 results from the previous DFT study by Román-Román and Zicovich-Wilson, in which the relative energies were calculated for 14 all-silica zeolites (BEA, MEI, and α-cristobalite were not considered in that work).[23] While the individual results differ considerably in some instances, PBE0-D2 and PBEsol-TS are similar in their tendency to overestimate the relative energies systematically. This is also reflected in the very similar overall errors, which are included in Table IX. Furthermore, PBE0-D2 overestimates the unit cell volumes much more significantly than either of the PBEsol-based approaches. These are quite interesting findings, as the rather accurate prediction of structural parameters and relative energies by PBEsol (or PBE) in conjunction with the D2 dispersion correction is deteriorated when a pure-GGA functional is replaced by a more elaborate hybrid functional (which, as mentioned above, sits on a higher rung of "Jacob's Ladder"). Although we cannot trace the origin of this behavior in the context of the present study, it could indicate that the excellent performance of PBEsol-D2 is, to some extent, the result of a fortuitous cancellation of errors.

TABLE IX. Overall errors in relative energies obtained with PBEsol-D2 and PBEsol-TS functionals and comparison to PBE0-D2.[23] The largest individual errors found among all systems are also given: LSE± = largest signed positive/negative error; LRE± = largest relative positive/negative error.

	PBEsol-D2	PBEsol-TS	PBE0-D2
MSE (kJ mol^{-1})	+0.69	+2.35	+2.59
MAE (kJ mol^{-1})	1.08	2.42	2.60
LSE+ (kJ mol^{-1})	+2.20 (FER)	+3.91 (STT)	+4.40 (AFI)
LSE– (kJ mol^{-1})	–1.93 (MTW)	–0.61 (MTW)	–0.10 (ISV)
RMSE (%)	15.4	30.9	34.7
LRE+ (%)	+33.4 (FER)	+57.2 (FER)	+65.2 (FER)
LRE– (%)	–22.2 (MTW)	–7.0 (MTW)	–0.7 (ISV)

C. Additional aspects: The role of the scaling factor and extension to charged-framework compounds

Having assessed the performance of PBEsol-D2 and PBEsol-TS in detail, it is useful to consider two additional points. The first one concerns the influence of the scaling factor used in the dispersion correction scheme. As described above, the scaling factors s_r of PBEsol-D2 and PBEsol-TS were determined by minimising the error with respect to high-level CCSD(T) reference data for the S22 benchmark set of organic dimers. Clearly, it is not advisable to redetermine the scaling factor on the purely empirical basis of a comparison to experimental data. Nevertheless, it might be useful to assess how the agreement in structural parameters and relative energies changes when the scaling factor is modified. Additional calculations for a subset of structures using the PBEsol-TS functional with varying values of s_r showed that the best agreement in lattice parameters is observed when the scaling factor is slightly reduced (to s_r = 1.02). However, this leads to even larger deviations in the relative energies, for which a larger scaling factor in the range of 1.15 would lead to an optimal agreement. Thus, it is apparent that no simple adjustment in either direction affords perfect agreement for both structures and energetics simultaneously. In this context, it is worth noting that previous studies found a pronounced overestimation of the cohesive energies by the TS scheme for ionic compounds, which was explained with a tendency of the Hirshfeld partitioning scheme to deliver too large C_6 coefficients for cations.[71] It was shown that a replacement of the original Hirshfeld method by an iterative Hirshfeld (HI) partitioning of the DFT electron density greatly improves the performance for ionic solids. Since the Si–O bond can be best described as having an intermediate character between the ionic and covalent limits,[78] it is not surprising that the TS scheme also exaggerates the contribution of dispersion interactions in purely siliceous materials, resulting in the systematic overestimation of relative energies observed above. Altogether, it appears likely that switching to the TS/HI approach, rather than modifying the scaling factor

s_r, would be a more promising strategy to improve the accuracy of PBEsol-TS for relative energies.

Second, a comment should be made regarding the transferability of the findings of present work to charged-framework compounds, as most zeolites that are relevant to applications consist of a negatively charged framework whose charge is balanced by protons or extra-framework cations. As we have seen above, the TS dispersion correction scheme has some problems for ionic solids due to the overestimation of the C_6 coefficients for cations. Since the D2 scheme uses only a single set of dispersion coefficients, which were derived for neutral atoms, its application for charged-framework compounds is also likely to be problematic. For example, several studies have shown that a combination of the PBE functional with the D2 dispersion correction systematically overestimates the interaction energies of small molecules with cationic zeolites.[79–81] Additional complications are likely to arise for zeolites exchanged with transition metal cations, which are used in many catalytic applications. Here, it has been shown that GGA-type functionals do not provide an accurate description of the electronic structure and that the—computationally more demanding—hybrid functionals are a better choice.[82] On the basis of these known issues, it can be anticipated that both PBEsol-D2 and PBEsol-TS will not perform as well for charged-framework zeolites as for their neutral-framework counterparts. While future benchmarking studies addressing charged-framework compounds could draw from a rich body of experimental structure data for ordered, dense materials (like feldspars and other silicate minerals), the extension to aluminosilicate zeolites is hampered by the frequent occurrence of mixed T site occupancies and cation disorder in these materials. Although new approaches to generate ordered structure models from disordered experimental structures may prove very useful in this respect,[83,84] the necessity to consider a sufficiently large set of different, representative structure models would significantly increase the computational cost.

IV. CONCLUSIONS

From the benchmarking against experimental structure data, we can conclude that both PBEsol-D2 and PBEsol-TS combine an excellent prediction of the lattice parameters—improving over the performance of PBE-TS, the best functional found in our previous study—with a reasonably accurate prediction of T–O bond distances and T–O–T angles, for which they perform much better than all PBE-based approaches and are on par with the uncorrected PBEsol functional. Among the two, PBEsol-TS is slightly better for lattice parameters, whereas there is no appreciable difference for bond lengths and angles.

Since the DFT-optimized structures were compared to experimental data that was—in most cases—obtained at room temperature, it could be argued that the agreement is to some extent fortuitous because errors in the DFT approach might compensate for the effect of temperature on lattice parameters and bond distances. To rule out this possibility, the structural parameters obtained from DFT were also compared to low-temperature lattice parameters and to T–O bond lengths that were corrected for temperature effects using a simple rigid bond model. While this analysis could only be performed for a subset of structures due to the lack of available experimental data, it was clear that the overall agreement between DFT and experiment improved if temperature effects were accounted for. This corroborates the suitability of PBEsol-D2 and PBEsol-TS to give accurate 0 K structures. In order to expand on the present findings, calculations should be combined with low-temperature diffraction experiments on high-quality calcined samples, e.g., using neutron radiation. In the view of recent developments to predict the thermal expansion from DFT calculations,[85,86] it might be particularly rewarding to address the negative thermal expansion that is often observed in neutral-framework zeotypes with a combination of computations and experiments.

A thorough comparison of the relative energies derived from the dispersion-corrected DFT calculations to experimentally available enthalpies of transition delivered excellent agreement for the PBEsol-D2 functional, whereas PBEsol-TS showed a systematic tendency to overestimate the relative energies. Since the calculations considered a fairly large number of all-silica zeolites, which extend across a range of framework densities from 13 to 20 T atoms per 1000 Å^3, it can be stated with confidence that PBEsol-D2 will also be suitable for predictive purposes. Notably, it performs better than the PBE0-D2 functional used in a previous study[23] and similarly well as a recent force field that was developed specifically for the prediction of the structure, energetics, and vibrational properties of all-silica zeolites.[87] It would be a logical next step to extend the prediction of relative energies to aluminophosphates. However, the few experimental datapoints that are available show no correlation between the enthalpy of transition and framework density, in contrast to the well-established relationships for all-silica zeolites.[31] This counterintuitive behavior can possibly be attributed to the presence of small amounts of water in the samples; however, it appears that this issue has not yet been fully resolved. At present, we consider the experimental data to be insufficiently reliable to serve as a benchmark for the calculations.

The excellent prediction of relative energies by PBEsol-D2 is somewhat surprising when it is considered that the D2 approach uses a fixed set of C_6 coefficients derived for neutral atoms, thus not accounting for the partly ionic character of the Si–O bond. While the good performance across the board of systems studied gives confidence in the robustness of the approach, it is likely that PBEsol-D2 benefits to some extent from a cancellation of errors. In any case, the present results may serve as a benchmark for the performance of relatively low-level DFT methods, GGA functionals with an empirical pairwise dispersion correction term, against which the possible improvements that can be gained from using more evolved approaches can be measured.

SUPPLEMENTARY MATERIAL

See supplementary material for additional tables reporting results for individual systems, further technical information on the DFT calculations, and CIF files of all DFT-optimised structures.

ACKNOWLEDGMENTS

M.F. is grateful to Professor Dr. Andreas Lüttge and Dr. Rolf Arvidson (Marum, Bremen) for generous access to the Asgard cluster, on which the DFT calculations were run, and to Filip Formalik (Wrocław) for a critical reading of the manuscript. M.F. is funded by the Central Research Development Funds (CRDF) of the University of Bremen (Funding line 04—Independent Projects for Post-Docs).

[1] L. Goerigk and S. Grimme, Phys. Chem. Chem. Phys. **13**, 6670 (2011).
[2] T. Risthaus and S. Grimme, J. Chem. Theory Comput. **9**, 1580 (2013).
[3] K. Remya and C. H. Suresh, J. Comput. Chem. **34**, 1341 (2013).
[4] J. Rezáč and P. Hobza, Chem. Rev. **116**, 5038 (2016).
[5] E. Brémond, M. Savarese, N. Q. Su, A. J. Pérez-Jiménez, X. Xu, J. C. Sancho-García, and C. Adamo, J. Chem. Theory Comput. **12**, 459 (2016).
[6] J. Binns, M. R. Healy, S. Parsons, and C. A. Morrison, Acta Crystallogr., Sect. B: Struct. Sci., Cryst. Eng. Mater. **70**, 259 (2014).
[7] D. J. Carter and A. L. Rohl, J. Chem. Theory Comput. **10**, 3423 (2014).
[8] F. Tran, R. Laskowski, P. Blaha, and K. Schwarz, Phys. Rev. B **75**, 115131 (2007).
[9] P. Haas, F. Tran, and P. Blaha, Phys. Rev. B **79**, 085104 (2009).
[10] R. Demichelis, B. Civalleri, M. Ferrabone, and R. Dovesi, Int. J. Quantum Chem. **110**, 406 (2010).
[11] R. Demichelis, B. Civalleri, P. D'Arco, and R. Dovesi, Int. J. Quantum Chem. **110**, 2260 (2010).
[12] M. De la Pierre, R. Orlando, L. Maschio, K. Doll, P. Ugliengo, and R. Dovesi, J. Comput. Chem. **32**, 1775 (2011).
[13] D. Tunega, T. Bučko, and A. Zaoui, J. Chem. Phys. **137**, 114105 (2012).
[14] M. Råsander and M. A. Moram, J. Chem. Phys. **143**, 144104 (2015).
[15] F. Tran, J. Stelzl, and P. Blaha, J. Chem. Phys. **144**, 204120 (2016); e-print arXiv:1603.01504.
[16] J. P. Perdew, A. Ruzsinszky, L. A. Constantin, J. Sun, and G. I. Csonka, J. Chem. Theory Comput. **5**, 902 (2009).
[17] J. Perdew, A. Ruzsinszky, G. I. Csonka, O. A. Vydrov, G. E. Scuseria, L. A. Constantin, X. Zhou, and K. Burke, Phys. Rev. Lett. **100**, 136406 (2008).
[18] Z. Wu and R. Cohen, Phys. Rev. B **73**, 235116 (2006).
[19] J. P. Perdew, K. Burke, and M. Ernzerhof, Phys. Rev. Lett. **77**, 3865 (1996).
[20] B. Civalleri, C. M. Zicovich-Wilson, P. Ugliengo, V. R. Saunders, and R. Dovesi, Chem. Phys. Lett. **292**, 394 (1998).
[21] R. Astala, S. M. Auerbach, and P. A. Monson, J. Phys. Chem. B **108**, 9208 (2004).
[22] M. A. Zwijnenburg, F. Corá, and R. G. Bell, J. Phys. Chem. B **111**, 6156 (2007).
[23] E. I. Román-Román and C. M. Zicovich-Wilson, Chem. Phys. Lett. **619**, 109 (2015).
[24] M. Fischer, F. O. Evers, F. Formalik, and A. Olejniczak, Theor. Chem. Acc. **135**, 257 (2016).
[25] S. Grimme, J. Comput. Chem. **27**, 1787 (2006).
[26] A. Tkatchenko and M. Scheffler, Phys. Rev. Lett. **102**, 073005 (2009).
[27] H. Hay, G. Ferlat, M. Casula, A. P. Seitsonen, and F. Mauri, Phys. Rev. B **92**, 144111 (2015).
[28] C. Baerlocher and L. McCusker, Database of Zeolite Structures, 2012, See http://www.iza-structure.org/databases/.
[29] R. S. P. King, S. E. Dann, M. R. J. Elsegood, P. F. Kelly, and R. J. Mortimer, Chem. Eur. J. **15**, 5441 (2009).
[30] L. A. Villaescusa, P. A. Barrett, and M. A. Camblor, Chem. Mater. **10**, 3966 (1998).
[31] A. Navrotsky, O. Trofymluk, and A. A. Levchenko, Chem. Rev. **109**, 3885 (2009).
[32] I. Petrovic, A. Navrotsky, M. E. Davis, and S. I. Zones, Chem. Mater. **5**, 1805 (1993).
[33] K. Kihara, Eur. J. Miner. **2**, 63 (1990).
[34] M.-J. Díaz-Cabañas, P. A. Barrett, and M. A. Camblor, Chem. Commun. **1998**, 1881.
[35] J. A. Hriljac, M. M. Eddy, A. K. Cheetham, J. A. Donohue, and G. J. Ray, J. Solid State Chem. **106**, 66 (1993).
[36] J. E. Lewis, C. C. Freyhardt, and M. E. Davis, J. Phys. Chem. **100**, 5039 (1996).
[37] L. A. Villaescusa, P. Lightfoot, S. J. Teat, and R. E. Morris, J. Am. Chem. Soc. **123**, 5453 (2001).
[38] A. Corma, F. Rey, J. Rius, M. J. Sabater, and S. Valencia, Nature **431**, 287 (2004).
[39] B. Marler, A. Grünewald-Lüke, and H. Gies, Microporous Mesoporous Mater. **26**, 49 (1998).
[40] D. S. Wragg, R. Morris, A. W. Burton, S. I. Zones, K. Ong, and G. Lee, Chem. Mater. **19**, 3924 (2007).
[41] J. J. Williams, Z. A. D. Lethbridge, G. J. Clarkson, S. E. Ashbrook, K. E. Evans, and R. I. Walton, Microporous Mesoporous Mater. **119**, 259 (2009).
[42] B. P. Onac and H. S. Effenberger, Am. Mineral. **92**, 1998 (2007).
[43] R. M. Kirchner, R. W. Grosse-Kunstleve, J. J. Pluth, S. T. Wilson, R. W. Broach, and J. V. Smith, Microporous Mesoporous Mater. **39**, 319 (2000).
[44] M. Amri and R. I. Walton, Chem. Mater. **21**, 3380 (2009).
[45] M. P. Attfield and A. W. Sleight, Chem. Mater. **10**, 2013 (1998).
[46] M. Afeworki, D. L. Dorset, G. J. Kennedy, and K. G. Strohmaier, Chem. Mater. **18**, 1697 (2006).
[47] J. J. Pluth, J. V. Smith, and J. Faber, J. Appl. Phys. **57**, 1045 (1985).
[48] J. W. Richardson, J. V. Smith, and S. Han, J. Chem. Soc., Faraday Trans. **86**, 2341 (1990).
[49] N. J. Henson, A. K. Cheetham, and J. D. Gale, Chem. Mater. **8**, 664 (1996).
[50] J. M. Newsam, M. M. J. Treacy, W. T. Koetsier, and C. B. D. Gruyter, Proc. R. Soc. A **420**, 375 (1988).
[51] M. A. Camblor, A. Corma, and S. Valencia, Chem. Commun. **1996**, 2365.
[52] P. Lightfoot, D. A. Woodcock, M. J. Maple, L. A. Villaescusa, and P. A. Wright, J. Mater. Chem. **11**, 212 (2001).
[53] L. A. Villaescusa, P. A. Barrett, and M. A. Camblor, Angew. Chem., Int. Ed. **38**, 1997 (1999).
[54] M. A. Camblor, A. Corma, P. Lightfoot, L. A. Villaescusa, and P. A. Wright, Angew. Chem., Int. Ed. **36**, 2659 (1997).
[55] S. L. Lawton and W. J. Rohrbaugh, Science **247**, 1319 (1990).
[56] H. van Koningsveld, M. J. den Exter, J. H. Koegler, C. D. Laman, S. L. Njo, and H. Graafsma, in *Proceedings of the 12th International Zeolite Conference* (Cambridge University Press, 1999), pp. 2419–2424.
[57] H. van Koningsveld, J. C. Jansen, and H. van Bekkum, Zeolites **10**, 235 (1990).
[58] C. Deroche, "Experimentelle und rechnerische Analyse des Einbaus von Sorbatmolekülen in die Wirtsstrukturen der 12-Ring-Kanalsysteme ZSM-12 (MTW) und AlPO4-5 (AFI)," Ph.D. thesis, Ruhr-Universität Bochum, 1999.
[59] M. A. Camblor, A. Corma, M.-J. Diaz-Cabañas, and C. Baerlocher, J. Phys. Chem. B **102**, 44 (1998).
[60] M. A. Camblor, M.-J. Díaz-Cabañas, P. A. Cox, I. J. Shannon, P. A. Wright, and R. E. Morris, Chem. Mater. **11**, 2878 (1999).
[61] S. J. Clark, M. D. Segall, C. J. Pickard, P. J. Hasnip, M. I. J. Probert, K. Refson, and M. C. Payne, Z. Kristallogr. - Cryst. Mater. **220**, 567 (2005).
[62] P. Jurečka, J. Černý, P. Hobza, and D. R. Salahub, J. Comput. Chem. **28**, 555 (2007).
[63] G. I. Csonka, A. Ruzsinszky, J. P. Perdew, and S. Grimme, J. Chem. Theory Comput. **4**, 888 (2008).
[64] P. Jurečka, J. Šponer, J. Černý, and P. Hobza, Phys. Chem. Chem. Phys. **8**, 1985 (2006).
[65] S. Grimme, J. Antony, S. Ehrlich, and H. Krieg, J. Chem. Phys. **132**, 154104 (2010).
[66] C. Otero Areán, M. Rodríguez Delgado, P. Nachtigall, H. V. Thang, M. Rubeš, R. Bulánek, and P. Chlubná-Eliášová, Phys. Chem. Chem. Phys. **16**, 10129 (2014).
[67] K. Alexopoulos, M.-S. Lee, Y. Liu, Y. Zhi, Y. Liu, M.-F. Reyniers, G. B. Marin, V.-A. Glezakou, R. Rousseau, and J. A. Lercher, J. Phys. Chem. C **120**, 7172 (2016).
[68] R. Galvelis, B. Slater, A. K. Cheetham, and C. Mellot-Draznieks, CrystEngComm **14**, 374 (2012).
[69] F. L. Hirshfeld, Theor. Chim. Acta **44**, 129 (1977).
[70] E. R. Johnson and A. D. Becke, J. Chem. Phys. **123**, 024101 (2005).
[71] T. Bučko, S. Lebègue, J. Hafner, and J. G. Ángyán, J. Chem. Theory Comput. **9**, 4293 (2013).
[72] W. A. Al-Saidi, V. K. Voora, and K. D. Jordan, J. Chem. Theory Comput. **8**, 1503 (2012).
[73] R. T. Downs, G. V. Gibbs, K. L. Bartelmehs, and M. B. Boisen, Am. Mineral. **77**, 751 (1992).

[74]M. P. Attfield and A. W. Sleight, Chem. Commun. **1998**, 601.
[75]T. Carey, A. Corma, F. Rey, C. C. Tang, J. A. Hriljac, and P. A. Anderson, Chem. Commun. **48**, 5829 (2012).
[76]I. Bull, P. Lightfoot, L. A. Villaescusa, L. M. Bull, R. K. B. Gover, J. S. O. Evans, and R. E. Morris, J. Am. Chem. Soc. **125**, 4342 (2003).
[77]W. R. Busing and H. A. Levy, Acta Crystallogr. **17**, 142 (1964).
[78]G. V. Gibbs, K. M. Rosso, D. M. Teter, M. B. Boisen, and M. S. T. Bukowinski, J. Mol. Struct. **485-486**, 13 (1999).
[79]F. Göltl and J. Hafner, J. Chem. Phys. **134**, 064102 (2011).
[80]H. Fang, P. Kamakoti, P. I. Ravikovitch, M. Aronson, C. Paur, and D. S. Sholl, Phys. Chem. Chem. Phys. **15**, 12882 (2013).
[81]M. Fischer, M. Rodríguez Delgado, C. Otero Areán, and C. Oliver Duran, Theor. Chem. Acc. **134**, 91 (2015).
[82]F. Göltl and J. Hafner, J. Chem. Phys. **136**, 064503 (2012).
[83]M. Soeken, R. Drechsler, and R. X. Fischer, Z. Kristallogr. - Cryst. Mater. **231**, 107 (2016).
[84]K. Okhotnikov, T. Charpentier, and S. Cadars, J. Cheminf. **8**, 17 (2016).
[85]A. Erba, J. Chem. Phys. **141**, 124115 (2014).
[86]J. George, V. L. Deringer, A. Wang, P. Müller, U. Englert, and R. Dronskowski, J. Chem. Phys. **145**, 234512 (2016).
[87]Y. G. Bushuev and G. Sastre, Microporous Mesoporous Mater. **129**, 42 (2010).